

Modulation of oxygen production in Archaean oceans by episodes of Fe(II) toxicity

Elizabeth D. Swanner^{1*}, Aleksandra M. Mloszewska², Olaf A. Cirpka¹, Ronny Schoenberg¹, Kurt O. Konhauser² and Andreas Kappler¹

Oxygen accumulated in the surface waters of the Earth's oceans¹ and atmosphere² several hundred million years before the Great Oxidation Event between 2.4 and 2.3 billion years ago³. Before the Great Oxidation Event, periods of enhanced submarine volcanism associated with mantle plume events⁴ supplied Fe(II) to sea water. These periods generally coincide with the disappearance of indicators of the presence of molecular oxygen in Archaean sedimentary records⁵. The presence of Fe(II) in the water column can lead to oxidative stress in some organisms as a result of reactions between Fe(II) and oxygen that produce reactive oxygen species⁶. Here we test the hypothesis that the upwelling of Fe(II)-rich, anoxic water into the photic zone during the late Archaean subjected oxygenic phototrophic bacteria to Fe(II) toxicity. In laboratory experiments, we found that supplying Fe(II) to the anoxic growth medium housing a common species of planktonic cyanobacteria decreased both the efficiency of oxygenic photosynthesis and their growth rates. We suggest that this occurs because of increasing intracellular concentrations of reactive oxygen species. We use geochemical modelling to show that Fe(II) toxicity in conditions found in the late Archaean photic zone could have substantially inhibited water column oxygen production, thus decreasing fluxes of oxygen to the atmosphere. We therefore propose that the timing of atmospheric oxygenation was controlled by the timing of submarine, plume-type volcanism, with Fe(II) toxicity as the modulating factor.

Possible biological explanations for the slow tempo of atmospheric oxidation invoke limitations on the efficiency of early oxygenic photosynthesis, such as the toxicity of oxygen to the organisms who first produced it⁷, or that a paucity of key nutrients limited growth of oxygenic phototrophs in late Archaean sea water⁸. Iron is a key limiting nutrient for oxygenic photosynthesis in modern, oxic oceans, and enhanced Fe fluxes to the surface ocean are generally thought to have increased primary productivity over geologic time⁹. Coastal environments in the late Archaean experienced enhanced fluxes of Fe in its reduced, soluble form (Fe(II)) from upwelling sea water saturated with Fe(II) supplied from hydrothermal leaching of oceanic crust^{10,11}. In the absence of land plants in the late Archaean, a reasonable assumption is that most oxygen was produced or built up locally in coastal marine environments that experienced such upwelling^{5,12}, and oxygenic phototrophs would have experienced these Fe(II) fluxes. Nearly half of Earth's primary productivity, and hence its oxygen production, is today produced in the oceans¹³, and planktonic marine cyanobacteria, such as *Synechococcus* and *Prochlorococcus*, account for up to 25% of this number¹⁴. As previous work documented significant oxidative stress when planktonic cyanobacteria were

exposed to just 10 μM Fe(II) (ref. 6), an important constraint on late Archaean oxygen production is the fitness of planktonic cyanobacteria in producing oxygen in the presence of elevated Fe(II) fluxes.

We therefore used the planktonic marine cyanobacterium *Synechococcus* PCC 7002 to examine the effects of Fe(II) on oxygenic photosynthesis (see Supplementary Information for justification on use of this strain). We documented growth for this strain on anoxic medium supplied with different initial concentrations of Fe(II) (Fig. 1a). As oxygen was produced during growth, Fe(II) concentrations dropped owing to oxidation, and similar cell densities were ultimately achieved despite differing initial Fe(II) concentrations. However, the growth rates (μ ; d^{-1}) calculated from the initial part of the growth curves in Fig. 1a, when Fe(II) was still present in the medium, dropped significantly as initial Fe(II) concentrations increased to 180 μM and higher (Fig. 1b). Correspondingly, oxygen production was suppressed in cells grown at 300 μM Fe(II) or higher initial Fe(II) concentrations, evidenced by a significantly lower actinic yield, the ratio of variable fluorescence relative to maximum fluorescence (F_v/F_m ; ref. 15; Fig. 1d; for additional justification see Supplementary Information and Supplementary Fig. 1). An increase in Fe(II) concentrations from 10 to 100 μM in light-incubated cell suspensions caused intracellular reactive oxygen species (ROS) levels to double, and ROS levels quadrupled in the presence of 1,000 μM Fe(II) (Fig. 1c). These results link Fe(II) toxicity to enhanced intracellular concentrations of ROS, which results in a decrease in the efficiency of oxygenic photosynthesis, possibly due to inhibited repair of damaged photosystems¹⁶, and decreased growth rates.

To infer whether the Fe(II) toxicity we observed with *Synechococcus* PCC 7002 is common to diverse cyanobacteria, we screened microbial ecology data sets of circumneutral pH springs with persistent Fe(II) fluxes into sunlit, oxygenated surface environments (Table 1). All springs in which cyanobacteria were reported have less than 80 μM Fe(II) in source waters or within microbial mats. Springs with higher Fe(II) concentrations, in the range of several hundred μM Fe(II), are instead dominated by microaerophilic Fe(II)-oxidizers. The range of Fe(II) concentrations in which cyanobacteria inhabit these Fe(II)-rich environments is within the range of 7.5–55 μM Fe(II) at which we observed robust growth (Fig. 1a). The significant increase in intracellular ROS concentrations that we observed at 100 μM Fe(II) (Fig. 1c), the colonization of natural cyanobacteria in Fe(II)-rich springs with less than 80 μM Fe(II) (Table 1), and previous reports of Fe(II) toxicity for lagoonal cyanobacteria between 50 and 203 μM Fe(II) (ref. 17) lead us to propose that Fe(II) toxicity is common to cyanobacteria in the range of tens to hundreds of micromolar.

¹Department of Geosciences, University of Tübingen, Tübingen 72076, Germany. ²Department of Earth and Atmospheric Sciences, University of Alberta, Edmonton, Alberta T6G 2E3, Canada. *e-mail: elizabeth.swanner@ifg.uni-tuebingen.de

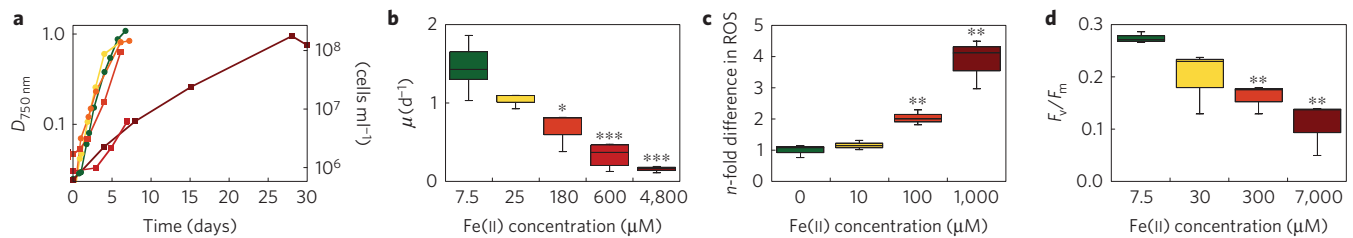


Figure 1 | Evidence for Fe(II) toxicity in *Synechococcus* PCC 7002. **a**, Attenuance ($D_{750\text{nm}}$; circles) of cells grown in the presence of 7.5 μM (green), 25 μM (yellow), or 55 μM (orange) Fe(II). Direct counts (squares), on a scale equivalent to the attenuation axis, of cells grown with 180 μM (dark orange), 600 μM (red) or 4,800 μM (brown) Fe(II). Standard error is generally smaller than the symbols. **b**, Cell-specific growth rates calculated from **a**, their biological replicates, and additional experiments. **c**, Intracellular ROS concentrations of cell suspensions incubated with Fe(II) in light. **d**, Actinic yield (F_v/F_m) of cells grown at different initial Fe(II) concentrations. Squares in **b–d** define the 25th and 75th quartile, horizontal lines the median, and the extending bars the minimum and maximum values of biological replicates. Asterisks denote the statistical significance: * for $P < 0.05$ (significant), ** for $P < 0.01$ (very significant), and *** for $P < 0.001$ (extremely significant). No asterisk indicates that differences are not statistically significant.

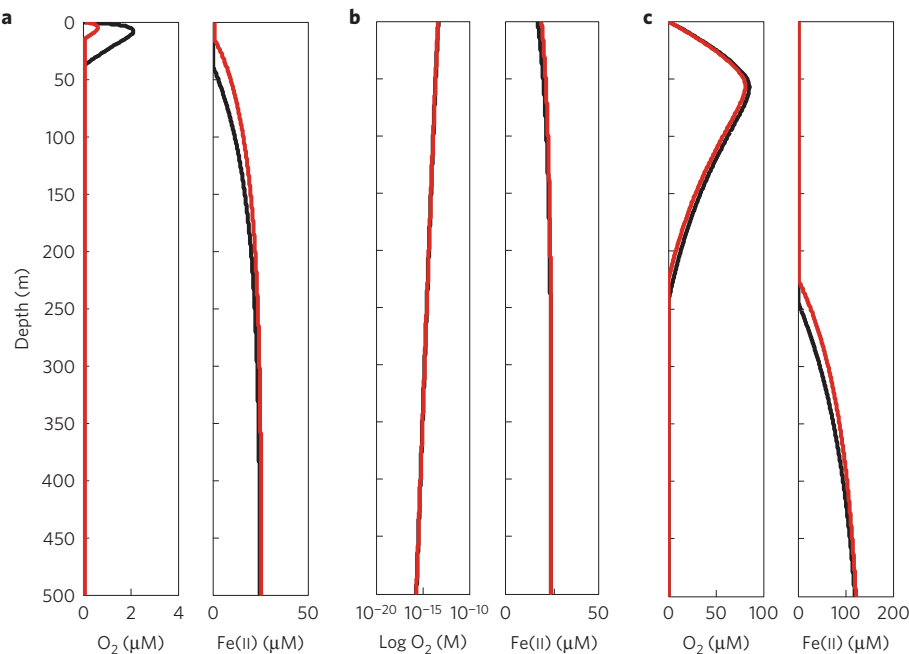


Figure 2 | Model of oxygen production modulated by Fe(II) toxicity. **a**, With deepwater Fe(II) concentrations of 25 μM and an upwelling rate of 95 m yr^{-1} , Fe(II) toxicity (red lines) reduces photosynthetic oxygen production so fluxes of oxygen to the atmosphere are only 36% of a scenario with no Fe(II) toxicity (black lines). **b**, With an enhanced upwelling rate (473 m yr^{-1}), high Fe(II) fluxes consume oxygen, resulting in negligible oxygen release to the atmosphere. **c**, Using an average global upwelling rate (4 m yr^{-1}), the Fe(II) flux cannot buffer oxygen release, either through chemical reaction or Fe(II) toxicity, even with enhanced deepwater Fe(II) concentrations (120 μM).

If Fe(II) is toxic to modern cyanobacteria, despite diverse strategies to detoxify ROS (ref. 6), it is possible that early cyanobacteria, or the organisms carrying out oxygenic photosynthesis during the late Archaean, also experienced Fe(II) toxicity, particularly if they had not yet acquired ROS detoxification mechanisms⁷. We therefore used a steady-state advective–diffusive transport model to address: whether Fe(II) would have reached the photic zone at ‘oxygen oases’ along upwelling zones; and the effect of Fe(II) toxicity on photosynthetic oxygen release and oxygen fluxes from the ocean to the atmosphere. The model allows Fe(II) to upwell from a deep basin and react with oxygen produced in the photic zone by oxygenic photosynthesis. Using an upwelling rate of 95 m yr^{-1} (ref. 18), and Fe(II) concentrations of 25 μM at depth in a 500 m basin, dissolved oxygen in surface waters reaches a maximum of 2 μM (Fig. 2a), similar to previously modelled values in Archaean ‘oxygen oases’ along upwelling zones¹² (see Supplementary Information for justification of parameters). However, when an inhibition parameter fit from the F_v/F_m data in Fig. 1d was invoked to simulate the effect of Fe(II)

toxicity, the rate of photosynthetic oxygen release was reduced to 80%, and the flux of oxygen to the atmosphere decreased to only 36% of values in the uninhibited scenario. Using higher estimates for deepwater Fe(II) concentrations, the effects of Fe(II) toxicity on oxygen release become more pronounced (Supplementary Fig. 2). In the model, enhanced upwelling rates (473 m yr^{-1} ; ref. 18), led to diminished oxygen production (Fig. 2b), and negligible fluxes of oxygen to the atmosphere ($< 10^{-17} \text{ M m}^2 \text{ s}^{-1}$). In this scenario, the enhanced reductant (that is, Fe(II)) flux, which consumes most oxygen produced, becomes more important than Fe(II) toxicity in modulating oxygen release. There is little effect of Fe(II) toxicity on photosynthetic oxygen production or release of oxygen to the atmosphere at average global upwelling rates (4 m yr^{-1}), as oxygen produced in the photic zone effectively buffers the much lower flux of Fe(II) from entering surface waters (Fig. 2c). In such a scenario, more analogous to an open-ocean setting, concentrations of tens of micromolar dissolved oxygen are achieved, implicating such sites as potential late Archaean ‘oxygen oases’ rather than previously

Table 1 | Microbial ecology of circumneutral pH, Fe(II)-rich springs or seeps.

Site type	Maximum dissolved Fe(II)	Cyanobacteria detected? Method?	Reference
Cold spring, Iceland	<1.7 μM	Yes. Molecular.	Ref. 30
Fuschna cold spring, Switzerland	16 μM	Yes. Molecular.	Ref. 31
Groundwater seep, Ohyato Park, Tokyo, Japan	37.6 μM	No. Molecular.	Ref. 32
Spring feeding Ogilvie Creek, Ontario, Canada	50 μM	Yes. Microscopy.	Ref. 33
Sambe hot spring, Shimane Prefecture, Japan	30–60 μM (total Fe)	Yes. Molecular.	Ref. 34
Chocolate Pots hot spring, Yellowstone NP, USA	50–200 μM at source; 50–80 μM within cyanobacterial mats	Yes. Microscopy.	Ref. 35; Ref. 36
Seep to Chalk River, Ontario, Canada	60–112 μM	No. Molecular.	Ref. 37
Seep to West Berry Creek, California, USA	156 μM (total Fe)	No. Molecular.	Ref. 38
Springs, Virginia, USA	127–177 μM ; 12.5–48.2 μM	No. Microscopy.	Ref. 39
Seeps to Contrary Creek, Virginia, USA	171 μM and 235 μM	Reportedly at low numbers.	Ref. 40
Seep, Aarhus, Denmark	250 μM	No. Microscopy.	Ref. 41
Jackson Creek, Indiana, USA	320–450 μM	No. Molecular.	Ref. 42

assumed coastal settings with higher upwelling rates. A caveat of this result is that nutrient limitation in such settings may have limited their productivity, and our model does not account for these limitations.

On the basis of experimental and ecological evidence for Fe(II) toxicity in cyanobacteria and the low oxygen fluxes modelled for periods of Fe(II) upwelling, we propose that plume-driven submarine volcanism and associated changes in sea level, circulation and deepwater reductant fluxes could have modulated late Archaean oxygen production. Numerous studies implicate episodic inputs of oxygen or a gradual rise of oxygen in the atmosphere and surface ocean before the Great Oxidation Event^{1,2,19,20} (GOE). Geochemical indicators, lasting perhaps tens of millions of years²¹, signal the periodic presence of dissolved oxygen in sea water along the slope of the Campbellrand/Malmani platform in South Africa between 2.7 and 2.5 billion years ago (Ga). During this interval, shifts towards heavier $\delta^{15}\text{N}$ values in shale organic carbon are consistent with onset of an oxic nitrogen cycle²², and contemporaneous shifts in sulphur isotopes indicating an oxidative sulphur cycle occur in coeval sediments in the Mount McRae shale in present-day northern Australia²³. Together with varying abundances of rhenium and molybdenum and Fe speciation data from shales that reflect cycling of these elements in bottom waters with some oxygen⁵, and coupled iron–molybdenum isotopic evidence for formation of Fe(III) (oxyhydr)oxide minerals in the water column²⁴, these indicators implicate oxygen production in pre-GOE coastal settings of the Transvaal and Hamersley basins.

In contrast, geochemical indicators for an oxygenated water column disappear from the Campbellrand/Malmani platform during major sea-level transgressions in which in Fe(II)-rich sea water blanketed the platform, slope and basin in iron formations^{10,21}. These shifts from carbonate to iron formation deposition are temporally linked to plume-driven submarine volcanism^{10,25}, which coincides with enhanced upwelling of Fe(II)-rich waters¹⁰. The main source of Fe(II) to late Archaean sea water is thought to have been upwelling hydrothermal fluids derived from oceanic crust altered at high temperature (>350 °C), as evidenced by positive Eu anomalies in carbonates of the about 2.46 to 2.67 Ga Campbellrand Subgroup of the Transvaal Supergroup deposited on the Kaapvaal Craton in South Africa¹¹. Evidence for 20–80 μM Fe(II) in the photic zone was previously inferred on the basis of the abundance of herringbone carbonate and the absence of micritic carbonate in the Gamohaian Formation of the Campbellrand Subgroup^{26,27}, as Fe(II) acts as an inhibitor to calcite precipitation. In further support of our assertion that upwelling Fe(II) modulated oxygen production, indicators from the sulphur isotope record for oxidation coincident

with the GOE (that is, the disappearance of mass independently fractionated sulphur) follow cessation of iron formation deposition associated with sea-level rise from plume-driven volcanism²⁵.

Evidence for Archaean atmospheric oxygen now extends as early as 3.0 Ga (refs 1,2), and if oxygen production is taken as a smoking gun signalling the initiation of oxygenic photosynthesis on Earth, then the tempo of atmospheric oxidation may reflect not when oxygenic photosynthesis first appeared, but rather shifts in patterns and styles of volcanism across the Archaean–Proterozoic boundary and GOE, such as waning plume-driven volcanism²⁵. Coupling the timing of oxygenation to events in secular rather than biological evolution is an old idea recapitulated⁷, with deference to the underlying role that a persistent, local supply of anoxic, Fe(II)-rich sea water could have had on regulating the activity and habitat of one of life's most prolific metabolisms. Central to this proposed series of events is the idea that input and distribution of Fe in the oceans was regulated by the timing and nature of crustal growth. The problem of disposing of oxygen, the toxic waste product of oxygenic photosynthesis, was not solved solely by using the geologic supply of Fe(II) as a sink⁷, but it also depended on periods of tectonic quiescence to sustain oxygen production in coastal habitats. More than the role of Fe as a nutrient⁹, Fe(II) toxicity regulates primary productivity in our model. Distinguishing the conditions under which Fe delivery to the oceans either restricted or stimulated primary productivity may well be critical in understanding the redox evolution and major element (C, S) budgets of Earth's oceans and atmosphere before, during and well after the GOE.

Methods

Synechococcus PCC 7002 was cultivated on anoxic Marine Phototroph (MP) medium with or without additional FeCl_2 at 24 °C with 12.8 $\mu\text{mol photons m}^{-2} \text{s}^{-1}$ (ref. 28). The trace element solution provided 7.5 μM Fe(II) to the medium. For growth experiments, 80 ml of medium was poured into 100 ml glass bottles (Schott AG) with a headspace of N_2/CO_2 (90:10). Growth was monitored by attenuation ($D_{750\text{nm}}$) measurements for cultures containing $\leq 100 \mu\text{M}$ Fe(II). For cultures with $> 100 \mu\text{M}$ Fe(II), cells were counted after fixation with paraformaldehyde and dissolution of the Fe(III) precipitates²⁸. Data for the counts in Fig. 1a represent the median value and standard error of counts on individual filters.

Attenuance readings were related to cells ml^{-1} (Fig. 1a) using a linear relationship determined between $D_{750\text{nm}}$ and direct microscopic counts. Growth rates (μ ; d^{-1}) were calculated during exponential growth phase from the linear portion of a semi-log plot of cells ml^{-1} (C) versus time (t ; days) using the equation:

$$\mu = (\ln C_2 - \ln C_1) / (t_2 - t_1) \quad (1)$$

An unpaired, two-tailed t -test (95% confidence interval) was used to determine whether the difference between a mean value obtained from biological replicates

performed at one concentration of Fe(II) was statistically significant from the mean value obtained with 7.5 μM or no added Fe(II) (for Fig. 1b–d). These results are reported in Supplementary Table 1. The statistical significance is reported as * for $P < 0.05$ (significant), ** for $P < 0.01$ (very significant), and *** for $P < 0.001$ (extremely significant). No asterisk indicates that differences are not statistically significant.

For Fe(II) quantification, samples containing $\geq 200 \mu\text{M}$ total Fe were diluted in anoxic 1 N HCl and analysed with 0.1% Ferrozine in 50% ammonium acetate. Samples containing $\leq 200 \mu\text{M}$ total Fe were reacted directly with Ferrozine for Fe(II) measurements. Absorption measurements at 563 nm were made after undiluted samples were centrifuged (19,000g) to pellet cells and Fe oxides.

The actinic yield (F_v/F_m) was determined on log-phase cultures grown at different Fe(II) concentrations with a Water PAM Chlorophyll Fluorometer (Heinz Walz). Approximately 2×10^6 cells ml^{-1} were washed and resuspended in a non-growth buffer at pH 6.8 (that is, MP medium lacking NH_4Cl , KH_2PO_4 , NaHCO_3 , trace elements, vitamin and supplements) for measurement.

The membrane-permeable indicator 5-(and-6)-chloromethyl-2',7'-dichlorodihydrofluorescein diacetate, acetyl ester (CM-H₂DCFDA) from Life Technologies GmbH was used for detection of intracellular ROS. A log-phase culture was collected by centrifugation and washed two times with a potassium phosphate buffer at pH 7. Cells were resuspended to a concentration of 2×10^7 cells ml^{-1} and degassed with N_2/CO_2 (90:10) in the dark. Stocks of anoxic FeCl_2 were added to final concentrations of 10 μM, 100 μM or 1,000 μM. The suspensions were incubated, shaking, at 25 μmol photons $\text{m}^{-2} \text{s}^{-1}$ for one hour. Cells were resuspended in fresh buffer with 5 μM CM-H₂DCFDA and incubated in the dark for 30 min. After resuspension in fresh buffer, the fluorescence emission at 519 nm (excitation at 490 ± 5 nm) was read using a FluoroMax-4 Spectrofluorometer (Horiba Europe GmbH). The fluorescence of non-stained cells and Fe minerals from identical treatments was subtracted.

We developed a steady-state advective–diffusive transport model coupled to the reaction of Fe(II) with oxygen:

$$\nu \frac{dc_{\text{Ox}}}{dz} - \frac{d}{dz} \left(D \frac{dc_{\text{Ox}}}{dz} \right) = r_{\text{photo}}^{\text{max}} \exp \left(-\frac{z}{z_{\text{photo}}} \right) - \gamma c_{\text{Ox}}^n c_{\text{Fe}}$$

$$\nu \frac{dc_{\text{Fe}}}{dz} - \frac{d}{dz} \left(D \frac{dc_{\text{Fe}}}{dz} \right) = -4\gamma c_{\text{Ox}}^n c_{\text{Fe}}$$

subject to

$$c_{\text{Ox}}(0) = c_{\text{Ox},0}$$

$$\left. \frac{dc_{\text{Fe}}}{dz} \right|_{z=0} = 0$$

$$\left. \frac{dc_{\text{Ox}}}{dz} \right|_{z=z_{\text{max}}} = 0$$

$$c_{\text{Fe}}(z_{\text{max}}) = c_{\text{Fe,max}}$$

in which c_{Ox} [mol l^{-3}] and c_{Fe} [mol l^{-3}] are the concentrations of dissolved oxygen and Fe(II), respectively, z [m] denotes depth, ν [m s^{-1}] is the upwelling velocity, D [$\text{m}^2 \text{s}^{-1}$] is the depth-dependent eddy diffusion coefficient, $r_{\text{photo}}^{\text{max}}$ [$\text{mol l}^{-3} \text{s}^{-1}$] is the maximum photosynthetic oxygen production rate, z_{photo} [m] and z_{max} [m] denote the penetration depth of light and the maximum depth of the model domain, respectively, γ [$\text{l}^{1/n} \text{mol}^{-n} \text{s}^{-1}$] is the pseudo-bimolecular rate coefficient of Fe(II) oxidation by oxygen, n [-] is the exponent of oxygen in the rate law, and $c_{\text{Ox},0}$ [mol l^{-3}] and $c_{\text{Fe,max}}$ [mol l^{-3}] are the fixed concentrations of oxygen and Fe(II) at the top and bottom of the modelled domain, respectively.

The eddy diffusion coefficient was estimated at each depth on the basis of diffusivities calculated from vertical profiles of the Black Sea²⁹:

$$D(z) = \begin{cases} 1 \times 10^{-5} \text{ [m}^2 \text{ s}^{-1}] - 1.6 \times 10^{-7} \text{ [m s}^{-1}] \times z & \text{if } z < 50 \text{ [m]} \\ 4 \times 10^{-8} \text{ [m}^2 \text{ s}^{-1}] \times z & \text{otherwise} \end{cases}$$

resulting in $D = 2 \times 10^{-6} \text{ m}^2 \text{ s}^{-1}$ at the pycnocline, assumed at 50 m depth. The electron transport rate (ETR) was calculated from F_v/F_m :

$$\text{ETR} = F_v/F_m \times \text{PAR} \times \text{AF} \times 0.5$$

where PAR is photosynthetically active radiation ($\mu\text{mol electrons m}^{-2} \text{s}^{-1}$), and AF is the absorption factor for the fraction of incident PAR absorbed by cells. The 0.5 term indicates that 50% of absorbed photons are used by Photosystem II. Our F_m/F_v data yield the following inhibition law:

$$\text{ETR} = \text{ETR}_{\text{max}} \times (c + 1 \times 10^{-6})^{-n}$$

where $n = 0.107 \pm 0.023$, and using linearized uncertainty propagation. All parameters applied in the model are detailed in Supplementary Table 2.

Received 14 August 2014; accepted 24 November 2014;
published online 5 January 2015

References

- Planavsky, N. J. *et al.* Evidence for oxygenic photosynthesis half a billion years before the Great Oxidation Event. *Nature Geosci.* **7**, 283–286 (2014).
- Crowe, S. A. *et al.* Atmospheric oxygenation three billion years ago. *Nature* **501**, 535–538 (2013).
- Bekker, A. *et al.* Dating the rise of atmospheric oxygen. *Nature* **427**, 117–120 (2004).
- Barley, M. E., Pickard, A. L. & Sylvester, P. J. Emplacement of a large igneous province as a possible cause of banded iron formation 2.45 billion years ago. *Nature* **385**, 55–58 (1997).
- Kendall, B. *et al.* Pervasive oxygenation along late Archean ocean margins. *Nature Geosci.* **3**, 647–652 (2010).
- Scholnick, S., Summerfield, T. C., Reyntman, L., Sherman, L. A. & Keren, N. The mechanism of iron homeostasis in the unicellular cyanobacterium *Synechocystis* sp. PCC 6803 and its relationship to oxidative stress. *Plant Physiol.* **150**, 2045–2056 (2009).
- Cloud, P. E. Jr Atmospheric and hydrospheric evolution on the primitive Earth: Both secular accretion and biological and geochemical processes have affected Earth's volatile envelope. *Science* **160**, 729–736 (1968).
- Kasting, J. F. What caused the rise of atmospheric O₂? *Chem. Geol.* **362**, 13–25 (2013).
- Martin, J. H. Glacial–interglacial CO₂ change: The iron hypothesis. *Paleoceanography* **5**, 1–13 (1990).
- Beukes, N. J. & Gutzmer, J. Origin and paleoenvironmental significance of major iron formations at the Archean–Paleoproterozoic boundary. *SEG Rev.* **15**, 5–47 (2008).
- Kamber, B. S. & Webb, G. E. The geochemistry of late Archean microbial carbonate: Implications for ocean chemistry and continental erosion history. *Geochim. Cosmochim. Acta* **65**, 2509–2525 (2001).
- Olson, S. L., Kump, L. R. & Kasting, J. F. Quantifying the areal extent and dissolved oxygen concentrations of Archean oxygen oases. *Chem. Geol.* **362**, 35–43 (2013).
- Field, C. B., Behrenfeld, M. J., Randerson, J. T. & Falkowski, P. Primary production of the biosphere: Integrating terrestrial and oceanic components. *Science* **281**, 237–240 (1998).
- Flombaum, P. *et al.* Present and future global distributions of the marine Cyanobacteria *Prochlorococcus* and *Synechococcus*. *Proc. Natl Acad. Sci. USA* **110**, 9824–9829 (2013).
- Campbell, D., Hurry, V., Clarke, A. K., Gustaffson, P. & Oquist, G. Chlorophyll fluorescence analysis of cyanobacterial photosynthesis and acclimation. *Microbiol. Mol. Biol. Rev.* **62**, 667–683 (1998).
- Nishiyama, Y., Allakhverdiev, S. I. & Murata, N. A new paradigm for the action of reactive oxygen species in the photoinhibition of photosystem II. *Biochim. Biophys. Acta* **1757**, 742–749 (2006).
- Demirel, S., Ustun, B., Aslim, B. & Suludere, Z. Toxicity and uptake of iron ions by *Synechocystis* sp. E35 isolated from Kucukcekmece Lagoon, Istanbul. *J. Hazard. Mater.* **171**, 710–716 (2009).
- Trabucho Alexandre, J. *et al.* The mid-Cretaceous North Atlantic nutrient trap: Black shales and OAEs. *Paleoceanography* **25**, PA4201 (2010).
- Anbar, A. D. *et al.* A whiff of oxygen before the great oxidation event? *Science* **317**, 1903–1906 (2007).
- Wille, M. *et al.* Evidence for a gradual rise of oxygen between 2.6 and 2.5 Ga from Mo isotopes and Re–PGE signatures in shales. *Geochim. Cosmochim. Acta* **71**, 2417–2435 (2007).
- Sumner, D. Y. & Beukes, N. J. Sequence stratigraphic development of the Neoproterozoic Transvaal carbonate platform, Kaapvaal, Craton, South Africa. *South Afr. J. Geol.* **109**, 11–22 (2006).
- Godfrey, L. V. & Falkowski, P. G. The cycling and redox state of nitrogen in the Archean ocean. *Nature Geosci.* **2**, 725–729 (2009).
- Kaufman, A. J. *et al.* Late Archean biospheric oxygenation and atmospheric evolution. *Science* **317**, 1900–1903 (2007).
- Czaja, A. D. *et al.* Evidence for free oxygen in the Neoproterozoic ocean based on coupled iron–molybdenum isotope fractionation. *Geochim. Cosmochim. Acta* **86**, 118–137 (2012).
- Barley, M. E., Bekker, A. & Krapež, B. Late Archean to early Paleoproterozoic global tectonics, environmental change and the rise of atmospheric oxygen. *Earth Planet. Sci. Lett.* **238**, 156–171 (2005).
- Sumner, D. Y. Carbonate precipitation and oxygen stratification in late Archean seawater as deduced from facies and stratigraphy of the Gamohaana and Frisco formations, Transvaal Supergroup, South Africa. *Am. J. Sci.* **297**, 455–487 (1997).
- Sumner, D. Y. & Grotzinger, J. P. Were kinetics of Archean calcium carbonate precipitation related to oxygen concentrations? *Geology* **24**, 119–122 (1996).

28. Wu, W. *et al.* Characterization of the physiology and cell-mineral interactions of the marine anoxygenic phototrophic Fe(II)-oxidizer *Rhodovulum iodolum*-implications for Precambrian Fe(II) oxidation. *FEMS Microbiol. Ecol.* **88**, 503–515 (2014).
29. Lewis, B. L. & Landing, W. M. The biogeochemistry of manganese and iron in the Black Sea. *Deep-Sea Res. A* **38** (suppl. 2), S773–S803 (1991).
30. Cockell, C. S., Kelly, L. C., Summers, S. & Marteinson, V. Following the kinetics: Iron-oxidizing microbial mats in cold Icelandic volcanic habitats and their rock-associated carbonaceous signature. *Astrobiology* **11**, 679–694 (2011).
31. Hegler, F., Lösekann-Behrens, T., Hanselmann, K., Behrens, S. & Kappler, A. Influence of seasonal and geochemical changes on the geomicrobiology of an iron carbonate mineral water spring. *Appl. Environ. Microbiol.* **78**, 7185–7196 (2012).
32. Kato, S., Chan, C., Itoh, T. & Ohkuma, M. Functional gene analysis of freshwater iron-rich flocs at circumneutral pH and isolation of a stalk-forming microaerophilic iron-oxidizing bacterium. *Appl. Environ. Microbiol.* **79**, 5283–5290 (2013).
33. James, R. E. & Ferris, F. G. Evidence for microbial-mediated iron oxidation at a neutrophilic groundwater spring. *Chem. Geol.* **212**, 301–311 (2004).
34. Mitsunobu, S. *et al.* Bacteriogenic Fe(III) (oxyhydr)oxides characterized by synchrotron microprobe coupled with spatially resolved phylogenetic analysis. *Environ. Sci. Technol.* **46**, 3304–3311 (2012).
35. Pierson, B. K., Paranteau, M. N. & Griffin, B. M. Phototrophs in high-iron-concentration microbial mats: Physiological ecology of phototrophs in an iron-depositing hot spring. *Appl. Environ. Microbiol.* **65**, 5474–5483 (1999).
36. Trouwborst, R. E., Johnston, A., Koch, G., Luther III, G. W. & Pierson, B. K. Biogeochemistry of Fe(II) oxidation in a photosynthetic microbial mat: Implications for Precambrian Fe(II) oxidation. *Geochim. Cosmochim. Acta* **71**, 4627–4643 (2007).
37. Gault, A. G. *et al.* Seasonal changes in mineralogy, geochemistry and microbial community of bacteriogenic iron oxides (BIOS) deposited in a circumneutral wetland. *Geomicrobiol. J.* **29**, 161–172 (2011).
38. Duckworth, O. W., Holmström, S. J. M., Pea, J. & Sposito, G. Biogeochemistry of iron oxidation in a circumneutral freshwater habitat. *Chem. Geol.* **260**, 149–158 (2009).
39. Rentz, J. A., Kraiyya, C., Luther, G. W. & Emerson, D. Control of ferrous iron oxidation within circumneutral iron mats by cellular activity and autocatalysis. *Environ. Sci. Technol.* **41**, 6084–6089 (2007).
40. Druschel, G. K., Emerson, D., Sutka, R., Suchecki, P. & Luther III, G. W. Low-oxygen and chemical kinetic constraints on the geochemical niche of neutrophilic iron(II) oxidizing microorganisms. *Geochim. Cosmochim. Acta* **72**, 3358–3370 (2008).
41. Emerson, D. & Revsbech, N. P. Investigation of an iron-oxidizing microbial mat community located near Aarhus, Denmark: Field studies. *Appl. Environ. Microbiol.* **60**, 4022–4031 (1994).
42. Roden, E. *et al.* The microbial ferrous wheel in a neutral pH groundwater seep. *Frontiers in Microbiology* **3** (2012).

Acknowledgements

This work was supported by an NSF IRFP fellowship to E.D.S. *Synechococcus* PCC 7002 was a gift from M. Eisenhut. D. Deubel, V. Hof, A. Klotz, E. Koeksoy, M. Maisch, S. Schmidt, C. Vogt and W. Wu assisted with experiments. This project benefited from helpful discussion with S. Eroglu, K. Forchhammer, S. J. Mojzsis, M. Mühe, M. Obst, A. Picard and B. Voelker.

Author contributions

E.D.S., O.A.C. and A.K. designed the research; E.D.S. performed the research, E.D.S., O.A.C. and A.K. analysed the data; R.S., A.M.M. and K.O.K. helped to develop key themes; E.D.S. wrote the paper, with major contributions from A.K., A.M.M., R.S. and K.O.K.

Additional information

Supplementary information is available in the [online version of the paper](#). Reprints and permissions information is available online at www.nature.com/reprints. Correspondence and requests for materials should be addressed to E.D.S.

Competing financial interests

The authors declare no competing financial interests.